Computational and Structural Biotechnology Journal 23 (2024) 1408–1417

Contents lists available at ScienceDirect

Computational and Structural Biotechnology Journal

journal homepage: www.elsevier.com/locate/csbj

Research article

Multiscale calculations reveal new insights into the reaction mechanism between KRAS^{G12C} and α, β-unsaturated carbonyl of covalent inhibitors

Xiao Yan [a,1], Chuanhua Qu [b,1], Qin Li [a], Lei Zhu [c], Henry H.Y. Tong [a], Huanxiang Liu [a,*], Qin Ouyang [c,*], Xiaojun Yao [a,*]

[a] Faculty of Applied Sciences, Macao Polytechnic University, Macao Special Administrative Region of China
[b] College of Pharmacy, National & Local Joint Engineering Research Center of Targeted and Innovative Therapeutics, Chongqing Key Laboratory of Kinase Modulators as Innovative Medicine, Chongqing University of Arts and Sciences, Chongqing 402160, China
[c] College of Pharmacy, Third Military Medical University, Shapingba, Chongqing 400038, China

ARTICLE INFO

Keywords:
KRAS^{G12C}
Covalent Inhibitors
QM/MM
DFT
Reaction Mechanism

ABSTRACT

Utilizing α,β-unsaturated carbonyl group as Michael acceptors to react with thiols represents a successful strategy for developing KRAS^{G12C} inhibitors. Despite this, the precise reaction mechanism between KRAS^{G12C} and covalent inhibitors remains a subject of debate, primarily due to the absence of an appropriate residue capable of deprotonating the cysteine thiol as a base. To uncover this reaction mechanism, we first discussed the chemical reaction mechanism in solvent conditions via density functional theory (DFT) calculation. Based on this, we then proposed and validated the enzymatic reaction mechanism by employing quantum mechanics/molecular mechanics (QM/MM) calculation. Our QM/MM analysis suggests that, in biological conditions, proton transfer and nucleophilic addition may proceed through a concerted process to form an enolate intermediate, bypassing the need for a base catalyst. This proposed mechanism differs from previous findings. Following the formation of the enolate intermediate, solvent-assisted tautomerization results in the final product. Our calculations indicate that solvent-assisted tautomerization is the rate-limiting step in the catalytic cycle under biological conditions. On the basis of this reaction mechanism, the calculated k_{inact}/k_i for two inhibitors is consistent well with the experimental results. Our findings provide new insights into the reaction mechanism between the cysteine of KRAS^{G12C} and the covalent inhibitors and may provide valuable information for designing effective covalent inhibitors targeting KRAS^{G12C} and other similar targets.

1. Introduction

Over the past decades, multiple mutations within the Kirsten Rat Sarcoma Viral Oncogene Homologue (KRAS) have been identified in numerous highly lethal cancers [1,2], including pancreatic ductal adenocarcinoma (PDAC) [3], non-small cell lung cancer [4] (NSCLC), and colorectal cancer [5] (CRC). Among the occurred mutations, KRAS^{G12C} mutation is high-frequently detected and closely associated with the occurrence of various cancers. KRAS^{G12C} mutant is also considered a promising and valid drug target for KRAS inhibitor development [6], breaking the undruggable history of KRAS [1]. AMG510 (also known as Sotorasib), the first drug in clinical use to target KRAS^{G12C} [7,8], contains α,β-unsaturated carbonyl functional group and can covalently bind to the residue CYS12, thereby locking KRAS^{G12C} in its inactive GDP-bound state [9]. However, the reaction mechanism between AMG510 and KRAS^{G12C} is still controversial, hindering further design and discovery of covalent inhibitors targeting KRAS^{G12C}.

Typically, the reaction between KRAS^{G12C} and AMG510 can be regarded as the addition of thiols to Michael acceptors. Scheme 1(a) shows the overall reaction process between thiols and α,β-unsaturated carbonyl group of the covalent inhibitors [10]. A key covalent bond is formed between C and S via Michael addition. Scheme 1(b) shows the general mechanism between α,β-unsaturated carbonyl and RSH under both solvent conditions and biological environments.

In the solution reaction condition, the exogenous base acts as a catalyst role, facilitating the catalytic cycle [11,12]. Generally, the overall reaction process can be divided into three steps [10,13,14]. Firstly, RSH is deprotonated by the exogenous base to form the thiolate

* Corresponding authors.
E-mail addresses: hxliu@mpu.edu.mo (H. Liu), ouyangq@tmmu.edu.cn (Q. Ouyang), xjyao@mpu.edu.mo (X. Yao).
[1] These authors contributed equally

https://doi.org/10.1016/j.csbj.2024.03.027
Received 16 November 2023; Received in revised form 29 March 2024; Accepted 29 March 2024
Available online 4 April 2024

anion RS^-. Then, a C-S bond is formed between RS^- and the α,β-unsaturated carbonyl group of the compound by nucleophilic addition [15,16]. Finally, the enolate anion is protonated by the BH^+ generated in step 1 to obtain the final product. However, the addition of thiols to the Michael acceptor in the biological system is different from the solution reaction conditions [17–22]. In the absence of an exogenous base, the base residues around the cysteine will generally act as a proton acceptor and facilitate the reaction. However, to our knowledge, not all proteins have appropriate base residues surrounding the cysteine, such as Bruton's tyrosine kinase [17,23], and $KRAS^{G12C}$. Mulholland et al. [17] suggested a possible mechanism between Bruton's tyrosine kinase and covalent inhibitors in the absence of appropriate base residue (Scheme 1b), the carbonyl group of the compound 2 would accept the proton from RSH to form the enolate intermediate. Subsequently, the key C-S bond in intermediate 5 was formed by nucleophilic addition between RS^- and enolate. It is still unknown if this mechanism is suitable for the reaction between $KRAS^{G12C}$ and its covalent inhibitors. Generally, the differences in the surrounding environment of various biological systems may lead to distinct reaction mechanisms. To explore the reaction mechanism of $KRAS^{G12C}$ with covalent inhibitors, several researches have been performed. For example, Nemukhin et al. [22] studied the reaction mechanism between the compound ARS-107 and $KRAS^{G12C}$. However, their research directly ignored the proton of SH in the reaction model, the C-S bond was formed via S^- addition to α,β-unsaturated carbonyl of ARS-107 compounds. Additionally, after the formation of the enolate anion intermediate, a proton from water coordinates with Mg^{2+} and saturates the enolate anion, resulting in the presence of a hydroxide anion in the final product. Keseru et. al [24] also adopted a similar strategy. Therefore, their unclosed and insufficient reaction cycle remains to be further discussed. To solve these problems, in this investigation, we explored the reaction mechanism between $KRAS^{G12C}$ and two covalent inhibitors (AMG510 and O5Y) by QM and

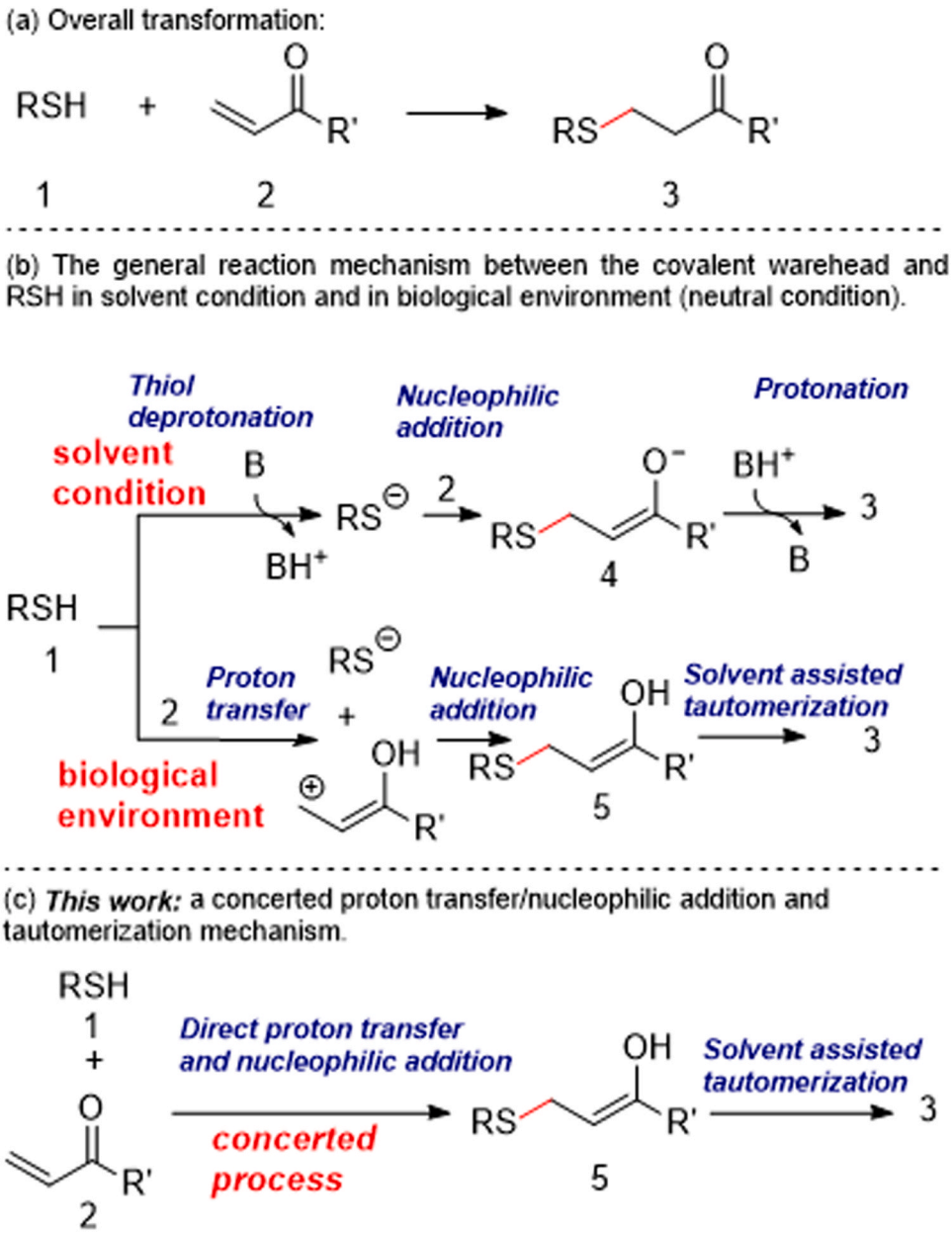

Scheme 1. The suggested general reaction mechanisms of thiols addition to α,β-unsaturated carbonyl group of covalent inhibitors. (a) the overall transformation of the reaction. (b) the general mechanism between the covalent warheads and RSH in solvent condition and biological environment. (c) a concerted proton transfer/nucleophilic addition and tautomerization mechanism.

QM/MM methods. AMG510 possesses a 6-member ring-linked warhead, while O5Y features a 4-member ring-linked warhead. To investigate the impact of warheads with different structures on the reaction process, both compounds were selected as research subjects.

Our calculated results show that the exogenous base HPO_4^{2-} can decrease the energy barrier of the nucleophilic addition step and facilitate the whole catalytic cycle in the solution reaction condition. However, in the absence of base residues in a biological environment, we proposed a concerted mechanism to form an enolate intermediate via the proton transfer/nucleophilic addition step as shown in Scheme 1(c). Based on this reaction mechanism, we subsequently calculated the k_{inact}/k_i values of covalent inhibitors to $KRAS^{G12C}$. The obtained results are in good agreement with the experimental findings, indicating the validity of our proposed model. The accurate reaction mechanism may provide valuable information for the design of safer and more selective covalent inhibitors targeting $KRAS^{G12C}$ and other similar targets.

2. Methods

Fig. 1 shows our overall research ideas for the reaction mechanism between $KRAS^{G12C}$ and two covalent inhibitors (AMG510 and O5Y). First, QM calculation was performed to explore the solution reaction mechanism of two covalent inhibitors with different warheads (AMG510 with warhead D and O5Y with warhead A shown in Fig. 1). Then, the molecular dynamics simulation was performed on the complexes of the covalent inhibitors with $KRAS^{G12C}$. After the conformational clustering analysis, two QM/MM models were constructed and investigated.

2.1. DFT calculation method

In the small models, all the initial structures including reactants, intermediates, transition states, and products were manually constructed via Gaussview 6.0 software [24] and then optimized freely at the B3LYP-D3 [25]/6–31G(d) [26] calculation level. In previous work, B3LYP is recommended to model cysteine reactivity [27] and can obtain a suitable electronic description consistent with higher-level methods [28]. The exchange-correlation function (B3LYP-D3) which can better describe noncovalent interaction [29] and keep consistent with experimental findings [30], was applied in this work. To validate that the optimized structure corresponds to a stationary point, a vibrational analysis was conducted. The intrinsic reaction coordinate [31] (IRC) path analysis was used to prove the energy profiles linking each transition state to two minima of the proposed intermediates. To give more accurate energy information, the single-point energy was calculated at B3LYP-D3/6–311++G(d,p) [32] level after preliminary structure optimization. Moreover, considering the influence of the solvent effect, all of the reactions were calculated with a polarizable continuum model [33,34] (PCM) at a dielectric constant of 78 (water). All of the density functional theory calculations were performed using the Gaussian 16 softpackage [35].

2.2. Classical MD simulations

To obtain reliable starting structures for QM/MM calculations, molecular dyanmics simulations were initially performed for the complexes of $KRAS^{G12C}$ and two covalent inhibitors. Both the crystal structures for AMG510 and O5Y with $KRAS^{G12C}$ have been reported with PDB ID 6OIM [36] and 6P8Y [37], respectively. In two crystal structures, the inhibitors are covalently bound to $KRAS^{G12C}$. But in the crystal structure of AMG510-$KRAS^{G12C}$, there are missing amino acid residues. At the same time, to minimize the structural difference between O5Y-$KRAS^{G12C}$ and AMG510-$KRAS^{G12C}$, the structure of AMG510-$KRAS^{G12C}$ was constructed by manually modifying the covalent ligand of O5Y-$KRAS^{G12C}$. For the sake of simplicity, the AMG510-$KRAS^{G12C}$ is simplified as AMG-$KRAS^{G12C}$ in this article. As shown in Fig. S1(a), two covalent inhibitors exhibit a similar binding pose in in $KRAS^{G12C}$. To ensure the conformation consistent with the AMG-$KRAS^{G12C}$ crystal structure, after manual modification, the constructed structure of AMG-$KRAS^{G12C}$ was compared with 6OIM [37]. The modelled AMG-$KRAS^{G12C}$ complex was aligned to 6OIM and the result was given in Fig. S1(b) with RMSD 0.962 Å. As can be seen in Fig. S1(b), the direction and location of AGM510 in the complex is well consistent with the AMG510 in 6OIM, proving that our modelled structure is reliable and can be used in the following molecular dynamics (MD) simulation. Classical MD simulations were carried out using the pmemd module of the GPU-accelerated Amber 20 package [38,39]. Force field parameters for the Mg^{2+} and GDP were generated by the MCPB.py [40] modules with the general Amber force field [41] (gaff). Besides, the Amber ff14SB [42] force field was used for the standard residues. The C12 residue, which is bonded to the covalent inhibitors O5Y and AMG510 in their complexes, was considered a non-standard residue. The relevant parameters for this residue were added using the Ambertools leap program. The complex was placed within a cubic TIP3P water box, ensuring that the complex was positioned approximately 15 Å away from the edges of the box. After the initial equilibrations, 300 ns MD simulations were performed. Following the MD simulation, the root mean square deviations (RMSDs) of the complexes (shown in Fig. S2) were calculated over the simulated time period to evaluate the convergence of the system. The clustering analysis was performed on the extracted conformations from the equilibrium trajectories by using the cpptraj module [43]. All of the conformations were clustered into 4 classifications for each system. As indicated in Table S1 and Fig. S3, cluster 1 accounted for approximately 80% of the conformations in both the O5Y-$KRAS^{G12C}$ complex and the AMG-$KRAS^{G12C}$ complex. Therefore, cluster 1 was chosen as the initial conformation for the subsequent QM/MM calculations.

2.3. QM/MM calculations

At present, QM/MM has been one of the most successful methods for investigating enzymatic reaction mechanisms [44–51]. In this study, the ONIOM [52] calculation method was applied for QM/MM calculations. During the QM/MM calculations, the complexes of $KRAS^{G12C}$ and water

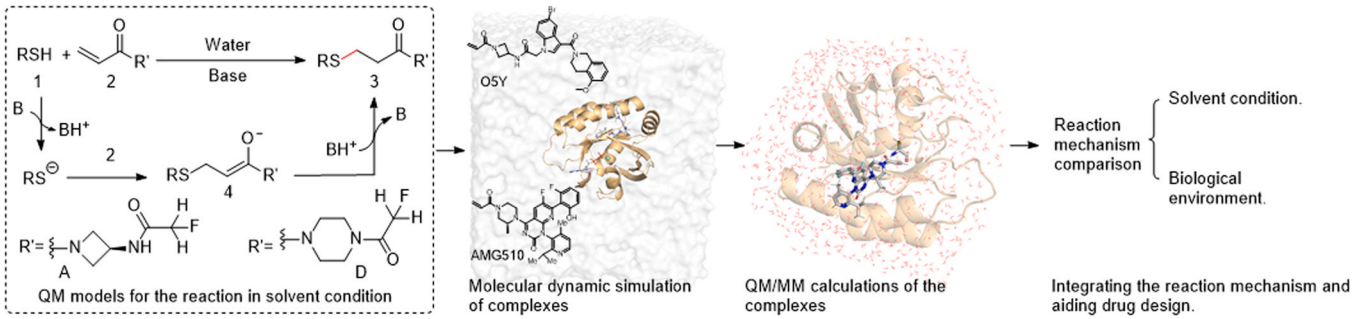

Fig. 1. Protocol for theoretical investigation of thiols addition to Michael acceptor.

molecules located at 4 Å around the complex were selected as the QM/MM region. The representative conformations of O5Y-KRAS^{G12C} and AMG-KRAS^{G12C} show that there are no extra residues near the C12 that can act as a proton acceptor (Fig. S4.). Besides, the analysis of H-bonds between inhibitors and KRAS^{G12C} were given in Table S2 and S3. The presence of low-frequency hydrogen bonds between the inhibitors and KRAS^{G12C} suggests that the surrounding residues of the covalent ligand are unable to form strong non-bonded interactions to stabilize the conformation of the inhibitor during the reaction. The strong non-bond interactions have been considered as one important factor to select QM region during QM/MM calculations [53,54]. As illustrated in Fig. S5, during the MD simulation of the AMG-KRAS^{G12C} complex, the average distance between the S atom of C12 and the O atom of the phosphate in GDP was measured to be 5.6 Å. During the MD simulation of O5Y-KRAS^{G12C} complex, the average distance between the S atom of C12 and the O atom of phosphate in GDP is 6.9 Å. Here, the phosphate group of GDP and K15 forms two hydrogen bonds but far away from the covalent ligand. Therefore, to save computational cost, the covalent inhibitors (O5Y and AMG510) and residue C12 were selected as the QM region as shown in Fig. 2. As results, for the O5Y-KRAS^{G12C} model, 5377 atoms were kept in whole QM/MM model, and 84 atoms were kept in the QM region. The charge, spin multiplicity of the QM region and the overall system were set to (0,1), (−7,1), respectively, for the reason of 7 Na^+ were added in the MD simulation. Similarly, in the AMG-KRAS^{G12C} model, 5238 atoms were kept for QM/MM calculation and 92 atoms were selected in the QM region. The charge, spin multiplicity of QM region and the whole system were set to (0,1) and (−7,1), respectively.

The keyword quadmac [55] was employed in the optimization, which performed a quadratic step in the coordinate between QM and MM atoms. To better keep the interaction of the Mg^{2+} and GDP, the phosphate group of GDP and Mg^{2+} were frozen in our QM/MM calculations. The gaff force field was applied to describe the MM region. The generated parameters of bond angle, bond distance, bond stretching and bond bending are given in supporting information. For the QM/MM model, the ONIOM(B3LYP/6–31 G(d):AMBER) level of the theory recommended by Lameira [27] was used in the overall structure optimization and frequency analysis of QM region. The B3LYP method has been used widely to discuss the enzymatic mechanisms [56–61] and can give reasonable results. The more precision single-point energy of the QM/MM model was calculated at ONIOM(B3LYP-D3/6–311 ++G(d,p): AMBER) level which can well recur the experimental results [30]. The default mechanical embedding was adopted in ONIOM calculation. And the IRC path analysis was employed to prove the energy profiles connecting each transition state to two minima of the proposed intermediates.

3. Results

3.1. The calculation results of small models suggest that exogenous base facilitates the catalytic cycle

As shown in Scheme 2, we first discussed the influence of different α,β-unsaturated carbonyl-containing warheads on the reaction process. The warhead screening experiment can simulate the reaction between thiol addition to the α,β-unsaturated carbonyl group and obtain the glutathione (GSH) half-times which can represent the reaction rate between covalent warheads and cysteine. Based on the screened structure of warhead, the inhibitor can be further designed. For example, the inhibitors O5Y and AMG510 contain a 4-member ring linked warhead A and 6-member ring linked warhead D, respectivly. Uncovering the reaction mechanism between covalent warhead and GSH may provide a guidance for the reaction mechanism of KRAS^{G12C} and its covalent inhibitors.

The warhead screening experimental condition was given in Scheme 2, the reactants GSH and covalent warhead were placed in the water solvent and the phosphate buffer was used as the base [62]. Victor et al. [63] found an intriguing phenomenon that covalent inhibitors A and D both with the same α,β-unsaturated carbonyl group have small difference in warhead structures, leading to different experimental GSH half-times. The GSH half-times of warhead A and D are about 100 mins and 200 mins respectively.

To explore why small difference in warhead structure leads to obvious difference in GSH half-times, the reaction mechanism between GSH and warheads was calculated by QM method. Two small reaction models were constructed and the halogen atom X was replaced by F in the calculation. In this reaction, the *p*H of the buffer solvent is 7.4 and the *p*Ka of -SH and two -COOH are 9.69, 1.98, and 3.49 [64], respectively, meaning that -SH can still be protonated under the reaction conditions. Furthermore, the concentration of HPO_4^{2-} ion is almost 2 to 4-fold excess of $H_2PO_4^-$ ion [65]. Hence, we mainly discussed the HPO_4^{2-} catalyzed reaction mechanism between GSH and compounds A or D. As

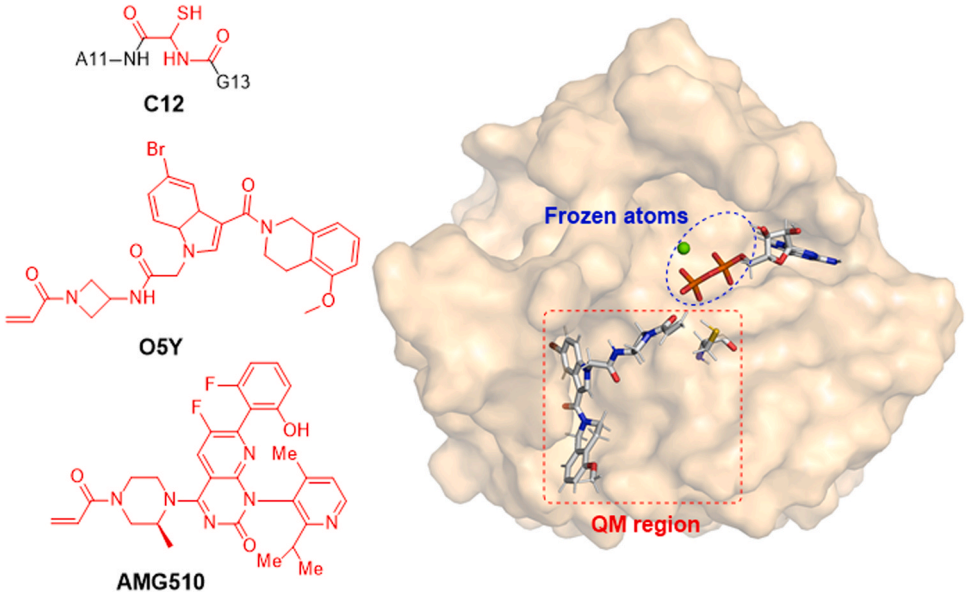

Fig. 2. The selected QM region and frozen atoms in QM/MM calculations. The QM region atoms was outlined by red color line.

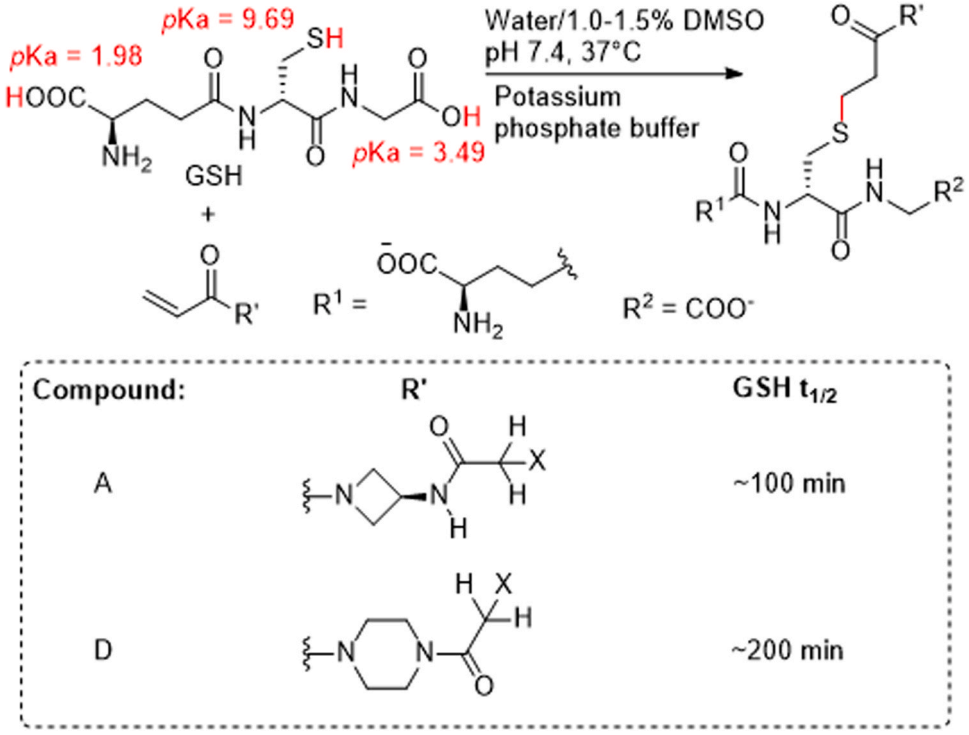

Scheme 2. Representative α,β-unsaturated carbonyl warhead, and its GSH half-life values.

shown in Fig. 3, GSH is firstly deprotonated by the HPO_4^{2-} to form the key intermediate thiol anion INT1. Subsequently, the thiol anion attacks the α,β-unsaturated carbonyl warhead A or D, which needs to overcome energy barrier of 16.5 and 17.0 kcal/mol, respectively. The calculated energy barrier is well consistent with Cee's work [62], indicating that our suggested mechanism is reasonable. Warhead A can form two hydrogen bonds with the thiol anion, leading to a related low energy barrier when compared with warhead D. Finally, the generated $H_2PO_4^-$ species can serve as a proton donor, facilitating the protonation of the unsaturated intermediate (INT2) and leading to the release of the final product.

We also discussed the case of $H_2PO_4^-$ as a base to catalyze the reaction process. The calculated results were given in Fig. S6. It can be seen that the $H_2PO_4^-$ as the base is thermodynamically unfavorable to the reaction with an energy barrier of 44.5 kcal/mol.

Proton transfer/nucleophilic addition in the absence of HPO_4^{2-} is also

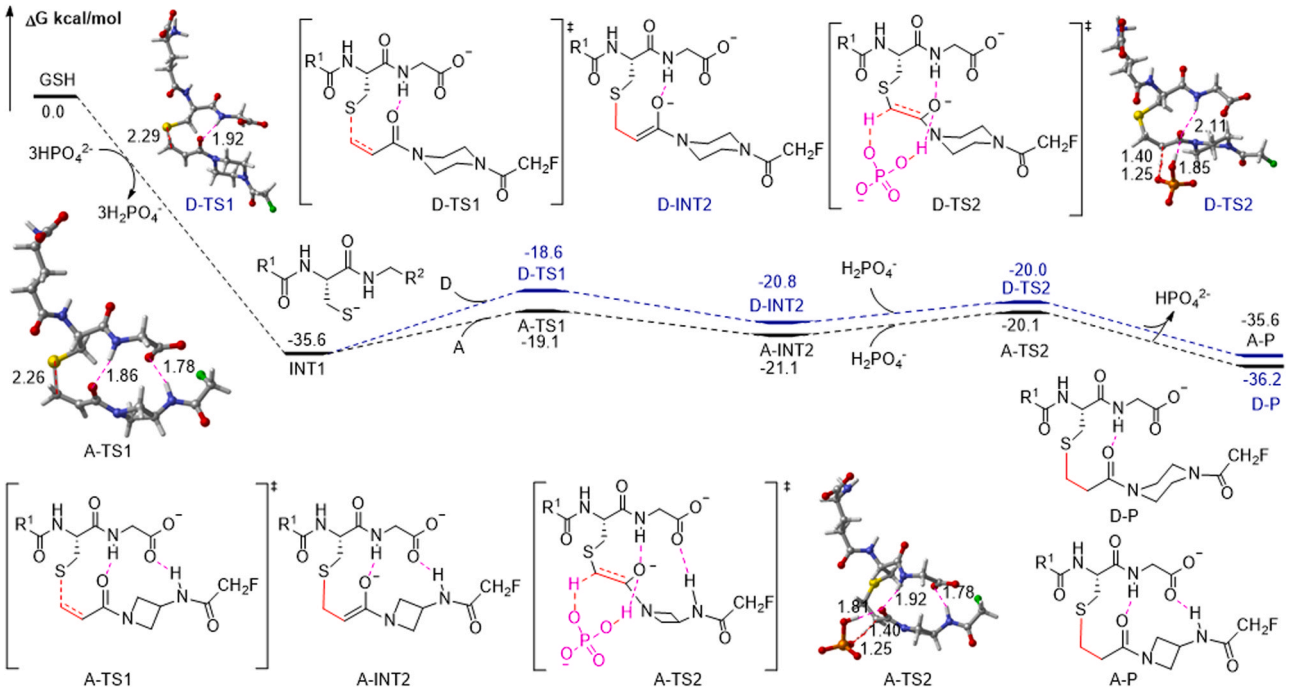

Fig. 3. HPO_4^{2-} catalyzed reaction mechanism between GSH and two warheads in buffer solvent. The energies are obtained at the B3LYP-D3/6–311++G(d,p)//B3LYP-D3/6–31G(d) level and are given in kcal mol^{-1} relative to the reactants.

investigated. As shown in Fig. 4, we find that 2-INT1 with warhead A or D may experience a concerted step to obtain the enolate intermediate when the base is absent in the proton transfer/nucleophilic attack step. The energy barrier of the proton transfer/nucleophilic addition are 28.0 (2-INT1→2-A-TS1) and 27.9 (2-INT1→2-D-TS1) kcal/mol, respectively. The IRC paths of the concerted step were given in Fig. S7 and Fig. S8. It is a relatively high energy barrier for the reaction along the concerted proton transfer/nucleophilic addition to obtain the enolate intermediates compared to the base catalyzed reaction. But in biological condition, without the proper residue as base, the reaction may adopt the concerted proton transfer/nucleophilic addition to get the intermediate.

In a word, our small model calculations proved the HPO_4^{2-} can reduce the energy barrier of the nucleophilic addition step and facilitate the reaction cycle. Moreover, without the catalysis of the base, the reaction may experience a concerted proton transfer/nucleophilic addition process to obtain the enolate intermediate. The proton transfer/nucleophilic addition transition state model can be employed in our subsequent QM/MM calculations.

3.2. The QM/MM calculations show that proton transfer and nucleophilic addition may adopt a concerted mechanism under biological reaction conditions, and solvent-assisted tautomerization is the rate-determining step

Based on the small reaction model, we further explored the reaction mechanism between $KRAS^{G12C}$ and covalent inhibitors based on QM/MM method. In general, thiol addition to the α,β-unsaturated carbonyl group of the covalent inhibitors may have four possible reaction mechanisms [17], as shown in Fig. 5, including direct proton transfer (Path A), solvent-assisted proton transfer (Path B), direct proton transfer followed by the nucleophilic addition and solvent-assisted tautomerization (Path C), and solvent assisted proton transfer/nucleophilic addition and tautomerization (Path D).

Based on this assumption, here, several possible reaction mechanisms between O5Y and $KRAS^{G12C}$ were explored based on QM/MM calculations. As shown in Fig. 6, our calculation results show that Path A and Path B need to overcome much higher energy barriers compared with Path C and D. Direct proton transfer and nucleophilic addition need to overcome an energy barrier of 48.3 kcal/mol (O5Y-TSA). Besides, water-assisted proton transfer and nucleophilic addition need to overcome an energy barrier of 33.1 kcal/mol (O5Y-TSB). The calculated results indicate the reaction between O5Y and $KRAS^{G12C}$ will not go through Path A and Path B. Relatively, in path C, the carbonyl group of O5Y acting as a proton acceptor can reduce the energy barrier of the proton transfer. The calculation results show that the proton transfer and nucleophilic addition may experience a concerted step to obtain the enolate intermediate O5Y-INTC. The reaction in path C didn't experience the ion pair state and the IRC path in Fig. S9 further proved the concerted process. In Path C, this step only needs to overcome an energy barrier of 4.6 kcal/mol (O5Y-TSC1). The suggested concerted mechanism is different from the previously reported stepwise process [17]. Following this step, water-assisted tautomerization, which needs to overcome an energy barrier of 18.7 kcal/mol (O5Y-INTC→O5Y-TSC2), is the rate-determining step of whole reaction process. Besides, we also discussed water-assisted proton transfer/nucleophilic addition (O5Y-TSD1, 6.8 kcal/mol). The energy of the transition state is 2.2 kcal/mol higher than O5Y-TSC1. Hence, the reaction along Path C to obtain the enolate intermediate is more favorable.

To further validate our proposed reaction mechanism, we also discussed the reaction mechanism between AMG510 and $KRAS^{G12C}$ (shown in Fig. 7). The reaction along Path A has to overcome an energy barrier of 52.9 kcal/mol (AMG-TSA). As for Path B, the energy barrier in the reaction is 31.8 kcal/mol (AMG-TSB). The Path C has a relative low energy barrier of 12.1 kcal/mol (AMG-TSC1). The IRC curve shown in Fig. S10 indicates the reaction does experience a concerted step to give the enolate intermediate. Similar with the O5Y-KRAS system, the water-assisted tautomerization (AMG-TSC2, 15.7 kcal/mol) is the rate-determining step in the whole reaction. Furthermore, in our investigation of solvent-assisted proton transfer (Path D), we observed that the involvement of a water molecule in the reaction did not significantly lower the energy barrier of the proton transfer/nucleophilic addition step. The energy barrier of the water-involved transition state (AMG-TSD1) was found to be 19.0 kcal/mol, which is 6.9 kcal/mol higher compared to the energy barrier of the direct proton transfer process (AMG-TSC1).

In addition to the four pathways discussed above, we also computed the reported mechanism suggested by previous work [22,24], where they used the thiol anion as the starting point of reaction. As depicted in Fig. S11, in Path E, cysteine 12 is deprotonated and the reaction proceeds with the thiol anion as the starting point, allowing for the formation of the C-S bond through nucleophilic attack. The energy barriers for C-S bond formation are calculated to be 6.3 kcal/mol (O5Y-TSE1) and 3.9 kcal/mol (AMG-TSE1), respectively. Subsequently, an intermediate is formed, which is then protonated by a water molecule. The protonation step is identified as the rate-determining step for the entire

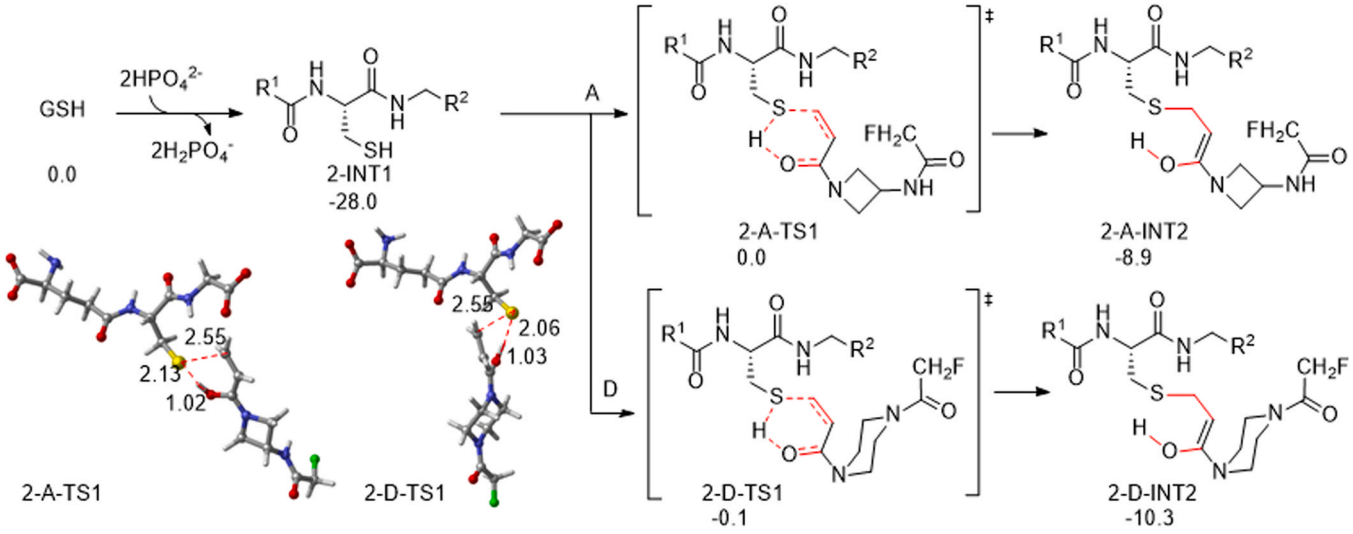

Fig. 4. Proton transfer/nucleophilic attack via a concerted process in the absence of proper base. The energies are obtained at the B3LYP-D3/6–311++G(d,p)//B3LYP-D3/6–31G(d) level and are given in kcal mol^{-1} relative to the reactants.

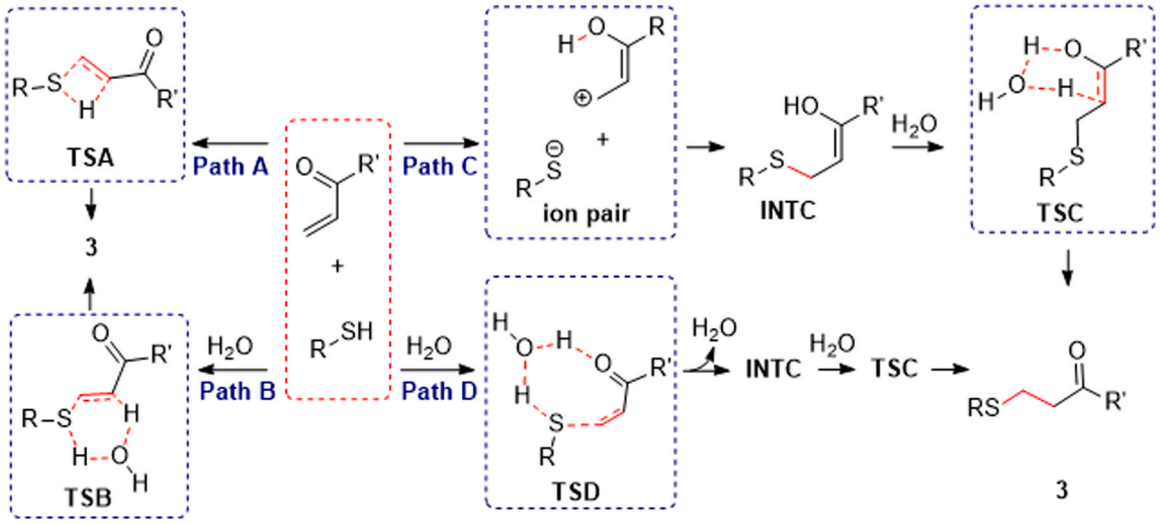

Fig. 5. Four possible reaction mechanisms between cysteine and the α,β-unsaturated carbonyl group of covalent inhibitors in neutral state. Path A. Direct proton transfer; Path B. Solvent-assisted proton transfer; Path C. Direct proton transfer followed by nucleophilic addition and solvent-assisted tautomerization; Path D. Solvent-assisted proton transfer, nucleophilic addition and tautomerization.

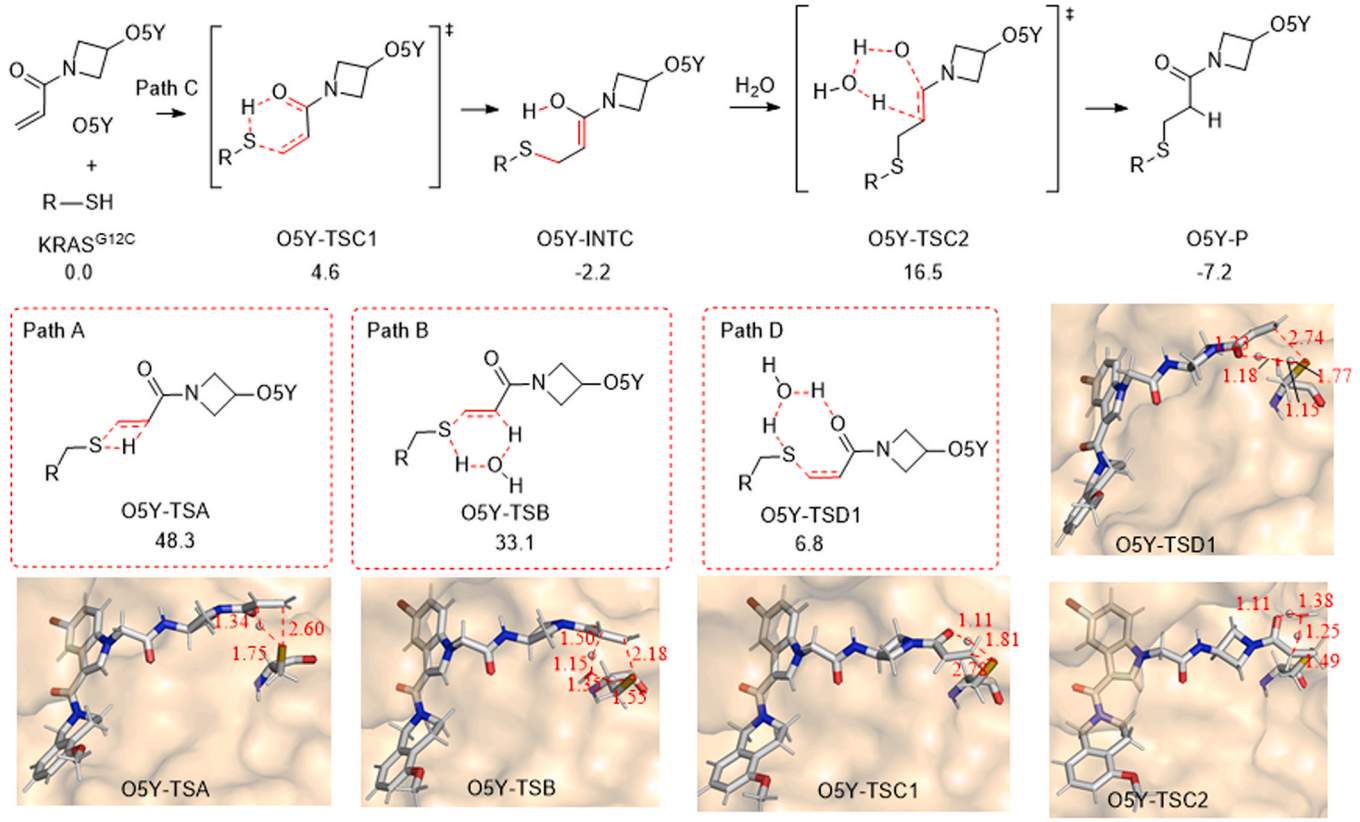

Fig. 6. The reaction mechanism between O5Y and $KRAS^{G12C}$. The energies are obtained at the B3LYP-D3/6–311++G(d,p):AMBER//B3LYP/6–31G(d):AMBER level and are given in kcal mol^{-1} relative to the reactants.

reaction. The activation energies for two inhibitors are determined to be 19.6 kcal/mol (O5Y-TSE2) and 24.5 kcal/mol (AMG-TSE2), respectively, which are higher than those of the reaction along Path C.

Based on the obtained results and discussions, it can be concluded that Path C is the most probable reaction mechanism between the investigated covalent inhibitors and $KRAS^{G12C}$. Compared to O5Y, AMG510 with a relatively large steric hindrance of six-member ring linker in the warhead may lead to a relatively high energy barrier in the proton transfer/nucleophilic addition step.

Our computational results show that proton transfer and nucleophilic addition may experience a concerted step to obtain the enolate intermediate, which is different from Mulholland's [17] research and can provide new insights into the thiol additions to Michael acceptors. Furthermore, invoking a water molecule to assist the proton transfer/nucleophilic addition is kinetically unfavorable. Finally, both two QM/MM models show that solvent-assisted tautomerization is the

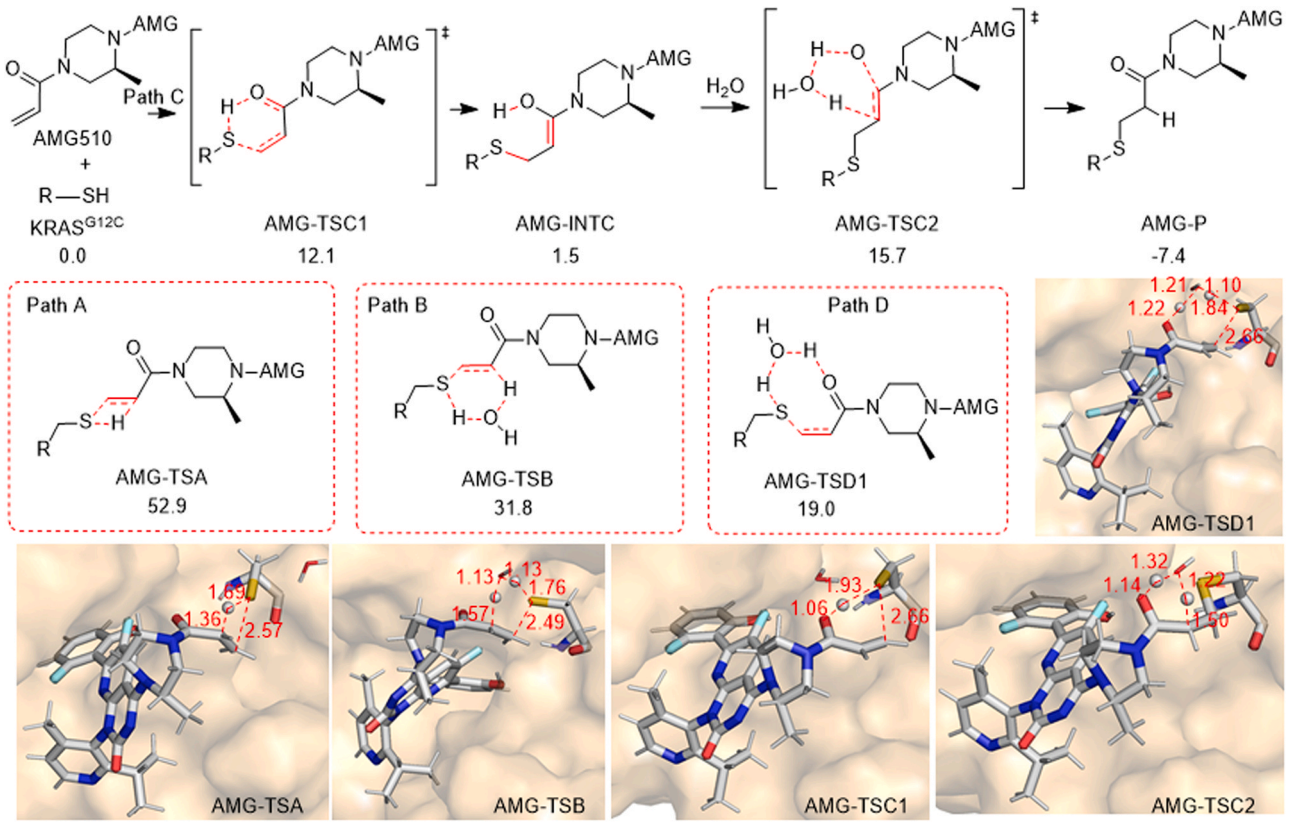

Fig. 7. The reaction mechanism between AMG510 and KRAS^{G12C}. The energies were obtained at the B3LYP-D3/6–311++G(d,p):AMBER//B3LYP/6–31G(d):AMBER level and were given in kcal mol^{-1} relative to the reactants.

rate-determining step which is consistent with the Mulholland's [17] report.

Based on the reaction mechanism, the k_{inact} and k_{inact}/k_i together with the activation energy ΔG for two inhibitors O5Y and AMG510 were calculated and given in Table 1. The k_{inact} refers to the rate constant for enzyme inactivation [66,67] which is calculated by using the Eyring equation [68], and the k_i is approximately equal to the experimental IC_{50} value [69]. The calculated k_{inact}/k_i for O5Y and AMG510 are 2304 and 10745, respectively, which are well consistent with the experimental values (2640 and 9900), further demonstrating that our proposed model, reaction mechanism and calculation methods are reliable.

4. Conclusions

In this study, in order to elucidate the reaction mechanism between KRAS^{G12C} and its covalent inhibitors, we successively explored the reaction mechanisms in solution and biological environments by employing DFT and QM/MM methods. The obtained results strongly suggest that the exogenous base $HPO4^{2-}$ plays a crucial role in facilitating the entire reaction cycle. Specifically, the presence of $HPO4^{2-}$ as a base can effectively reduce the energy barrier associated with nucleophilic attack in the solution environment. However, as shown in Fig. 8, in the absence of the base, the proton transfer/nucleophilic attack may experience a concerted step to form an enolate intermediate by using the carbonyl group of the warhead as proton acceptor.The biological reaction process also adopts a similar concerted mechanism. The rate-determining step of the whole reaction in biological condition is

Table 1
The calculated and experimental k_{inact} and k_{inact}/k_i values of two covalent KRAS inhibitors. The corresponding activation energy ΔG (calculated using transition state theory) is also given for comparison.

Inhibitor	ΔG (kcal/mol)	Inactivation rate, k_{inact} (s^{-1})	IC_{50} (μM)	k_{inact}/k_i (Exp, $M^{-1}s^{-1}$)	k_{inact}/k_i (Cal, $M^{-1}s^{-1}$)
O5Y	16.5	1.49	0.638 [63]	2640[63]	2304
AMG510	15.7	5.48	0.051 [8]	9900[8]	10745

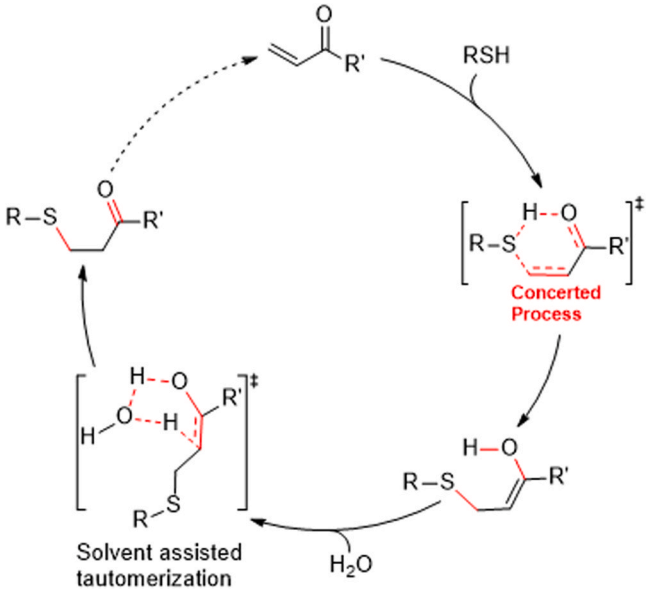

Fig. 8. Reaction mechanism of thiol addition to α,β-unsaturated carbonyl of covalent inhibitors in biological system.

solvent-assisted tautomerization which is consistent with previous research. Based on the proposed reaction mechanism, the calculated inactivation rate k_{inact} and k_{inact}/k_i values are well consistent with the experiment results, indicating that our suggested reaction mechanism is reliable.

By employing QM and QM/MM methods, the reaction mechanism between $KRAS^{G12C}$ and its covalent inhibitors was proposed. This reaction mechanism may also be suitable for other cysteine-targeting covalent inhibitors. For example, covalent inhibitors containing cyanoacrylamide, alanamide, and bicyclic [1.1.0] butylamine functional groups have α,β-unsaturated carbonyl moiety (as shown in Figure S11 [70]) and may have a reaction mechanism similar to the two covalent inhibitors we discussed. The suggested reaction mechanism can provide the important information for the design of more effective covalent drugs targeting $KRAS^{G12C}$ and other similar targets.

Author contributions

HX Liu, XJ Yao and Q Ouyang conceived and designed the research. X Yan, CH Qu and L Zhu performed and analyzed QM and QM/MM calculations. Q Li performed MD simulation and analysis. X Yan, HX Liu, HHY Tong, XJ Yao and Q Ouyang wrote and revised this manuscript. All authors have read and agreed to the final version of the manuscript.

Acknowledgements

This work is supported by the Science and Technology Development Fund, Macau, SAR (No. 0091/2022/A2) and Macao Polytechnic University (No. RP/ FCA-02 / 2023).

CRediT authorship contribution statement

Henry H. Y. Tong: Supervision. **Qin Ouyang:** Supervision, Writing – review & editing. **Xiaojun Yao:** Supervision, Writing – review & editing. **Huanxiang Liu:** Funding acquisition, Supervision, Writing – review & editing. **Xiao Yan:** Conceptualization, Formal analysis, Writing – original draft. **Chuanhua Qu:** Conceptualization, Formal analysis, Writing – review & editing. **Qin Li:** Conceptualization, Data curation, Writing – review & editing. **Lei Zhu:** Methodology.

Declaration of Competing Interest

The authors declare no competing financial interest.

Data Availability

The initial structures of the small reaction model were manually built by using GaussView 6.0 (https://gaussian.com/gaussview6), and the O5Y-$KRAS^{G12C}$ complex 6P8Y was downloaded from the RCSB Protein Data Bank (https://www.rcsb.org). All molecular simulations and analyses were performed by using Amber 20 (https://ambermd.org) software. The topology files of the molecular dynamic simulations are available from GitHub (https://github.com/Yaanshow/MD-Top-file). In addition, the Gaussian 16 software package (https://gaussian.com/) was used for ligand preparation, DFT and QM/MM calculations. All the calculated structures of key states in the small reaction model and the large reaction model were given in supporting information. All of the simulation parameters were given in the computation methods section. Corresponding structures were displayed by CYLview (http://www.cylview.org/).

Appendix A. Supporting information

Supplementary data associated with this article can be found in the online version at doi:10.1016/j.csbj.2024.03.027.

References

[1] Huang L, Guo Z, Wang F, Fu L. KRAS mutation: from undruggable to druggable in cancer. Signal Transduct Target Ther 2021;6:386.
[2] Lu S, Jang H, Gu S, Zhang J, Nussinov R. Drugging Ras GTPase: a comprehensive mechanistic and signaling structural view. Chem Soc Rev 2016;45:4929–52.
[3] Bailey P, Chang DK, Nones K, Johns AL, Patch A-M, Gingras M-C, et al. Genomic analyses identify molecular subtypes of pancreatic cancer. Nature 2016;531:47–52.
[4] Nadal E, Chen G, Prensner JR, Shiratsuchi H, Sam C, Zhao L, et al. KRAS-G12C mutation is associated with poor outcome in surgically resected lung adenocarcinoma. J Thorac Oncol 2014;9:1513–22.
[5] Prior IA, Hood FE, Hartley JL. The frequency of ras mutations in cancerras cancer statistics. Cancer Res 2020;80:2969–74.
[6] Lu S, Jang H, Muratcioglu S, Gursoy A, Keskin O, Nussinov R, et al. Ras conformational ensembles, allostery, and signaling. Chem Rev 2016;116:6607–65.
[7] Canon J, Rex K, Saiki AY, Mohr C, Cooke K, Bagal D, et al. , The clinical KRAS (G12C) inhibitor AMG 510 drives anti-tumour immunity. Nature 2019;575:217–23.
[8] Lanman BA, Allen JR, Allen JG, Amegadzie AK, Ashton KS, Booker SK, et al. Discovery of a covalent Inhibitor of KRAS(G12C) (AMG 510) for the treatment of solid tumors. J Med Chem 2020;63:52–65.
[9] Saiki AY, Gaida K, Rex K, Achanta P, Miguel TS, Koppada N, et al. Discovery and in vitro characterization of AMG 510–a potent and selective covalent small-molecule inhibitor of KRASG12C. Cancer Res 2019;79. 4484-4484.
[10] Roseli RB, Keto AB, Krenske EH. Mechanistic aspects of thiol additions to Michael acceptors: Insights from computations. WIREs Comput Mol Sci 2022;13.
[11] Wang C, Qi C. Mechanistic insights into N-or P-centered nucleophile promoted thiol–vinylsulfone Michael addition. Tetrahedron 2013;69:5348–54.
[12] Xi W, Wang C, Kloxin CJ, Bowman CN. Nitrogen-centered nucleophile catalyzed thiol-vinylsulfone addition, another thiol-ene "click" reaction. ACS Macro Lett 2012;1:811–4.
[13] Dmuchovsky B, Vineyard BD, Zienty FB. The mechanism of the base-catalyzed addition of thiols to maleic anhydride. J Am Chem Soc 1964;86:2874–7.
[14] De Maria P, Fini A. Kinetics of the nucleophilic addition of some aromatic thiols to aryl vinyl sulphones. J Chem Soc B: Phys Org 1971:2335–8.
[15] Mather BD, Viswanathan K, Miller KM, Long TE. Michael addition reactions in macromolecular design for emerging technologies. Prog Polym Sci 2006;31:487–531.
[16] Nair DP, Podgorski M, Chatani S, Gong T, Xi W, Fenoli CR, et al. The thiol-Michael addition click reaction: a powerful and widely used tool in materials chemistry. Chem Mater 2014;26:724–44.
[17] Voice AT, Tresadern G, Twidale RM, van Vlijmen H, Mulholland AJ. Mechanism of covalent binding of ibrutinib to Bruton's tyrosine kinase revealed by QM/MM calculations. Chem Sci 2021;12:5511–6.
[18] Capoferri L, Lodola A, Rivara S, Mor M. Quantum mechanics/molecular mechanics modeling of covalent addition between EGFR-cysteine 797 and N-(4-anilinoquinazolin-6-yl) acrylamide. J Chem Inf Model 2015;55:589–99.
[19] Grazioso G, Legnani L, Toma L, Ettari R, Micale N, De Micheli C. Mechanism of falcipain-2 inhibition by α, β-unsaturated benzo [1,4] diazepin-2-one methyl ester. J Comput-Aided Mol Des 2012;26:1035–43.
[20] Capoferri L, Lodola A, Rivara S, Mor M. Quantum mechanics/molecular mechanics modeling of covalent addition between EGFR–cysteine 797 and N-(4-anilinoquinazolin-6-yl) acrylamide. J Chem Inf Model 2015;55:589–99.
[21] Awoonor-Williams E, Rowley CN. Modeling the binding and conformational energetics of a targeted covalent inhibitor to Bruton's tyrosine kinase. J Chem Inf Model 2021;61:5234–42.
[22] Khrenova MG, Kulakova AM, Nemukhin AV. Proof of concept for poor inhibitor binding and efficient formation of covalent adducts of KRAS(G12C) and ARS compounds. Org Biomol Chem 2020;18:3069–81.
[23] Awoonor-Williams E, Rowley CN. Modeling the binding and conformational energetics of a targeted covalent inhibitor to Bruton's Tyrosine Kinase. J Chem Inf Model 2021;61:5234–42.
[24] Dennington R, Keith TA, Millam JM. GaussView 6.0. 16. Semichem Inc.: shawnee mission. KS, USA 2016:143–50.
[25] Grimme S, Antony J, Ehrlich S, Krieg H. A consistent and accurate ab initio parametrization of density functional dispersion correction (DFT-D) for the 94 elements H-Pu. J Chem Phys 2010;132:154104.
[26] Rassolov VA, Ratner MA, Pople JA, Redfern PC, Curtiss LA. 6-31G* basis set for third-row atoms. J Comput Chem 2001;22:976–84.
[27] Fekete A, Komáromi I. Modeling the archetype cysteine protease reaction using dispersion corrected density functional methods in ONIOM-type hybrid QM/MM calculations; the proteolytic reaction of papain. Phys Chem Chem Phys 2016;18:32847–61.
[28] Paasche A, Schirmeister T, Engels B. Benchmark study for the cysteine–histidine proton transfer reaction in a protein environment: Gas phase, COSMO, QM/MM approaches. J Chem Theory Comput 2013;9:1765–77.
[29] Kraus P, Frank I. Density functional theory for microwave spectroscopy of noncovalent complexes: a benchmark study. J Phys Chem A 2018;122:4894–901.
[30] Dos Santos AM, Oliveira ARS, da Costa CH, Kenny PW, Montanari CA, Varela JdJG, et al. Assessment of reversibility for covalent cysteine protease inhibitors using quantum mechanics/molecular mechanics free energy surfaces. J Chem Inf Model 2022;62:4083–94.
[31] Gonzalez C, Schlegel HB. An improved algorithm for reaction path following. J Chem Phys 1989;90:2154–61.
[32] Frisch MJ, Pople JA, Binkley JS. Self-consistent molecular orbital methods 25. Supplementary functions for Gaussian basis sets. J Chem Phys 1984;80:3265–9.

[33] Miertuš S, Scrocco E, Tomasi J. Electrostatic interaction of a solute with a continuum. A direct utilizaion of AB initio molecular potentials for the prevision of solvent effects. Chem Phys 1981;55:117–29.
[34] Miertus S, Tomasi J. Approximate evaluations of the electrostatic free energy and internal energy changes in solution processes. Chem Phys 1982;65:239–45.
[35] Frisch, M. ; Trucks, G. ; Schlegel, H. ; Scuseria, G. ; Robb, M. ; Cheeseman, J. et al. , Gaussian 16 Revision C. 01. 2016; Gaussian Inc. Wallingford CT 2016, 421.
[36] Canon J, Rex K, Saiki AY, Mohr C, Cooke K, Bagal D, et al. The clinical KRAS (G12C) inhibitor AMG 510 drives anti-tumour immunity. Nature 2019;575:217–23.
[37] Shin Y, Jeong JW, Wurz RP, Achanta P, Arvedson T, Bartberger MD, et al. Discovery of N-(1-Acryloylazetidin-3-yl)-2-(1H-indol-1-yl) acetamides as Covalent Inhibitors of KRASG12C. ACS Med Chem Lett 2019;10:1302–8.
[38] Salomon-Ferrer R, Götz A, Poole D, Le Grand S, Walker R. Routine microsecond molecular dynamics simulations with Routine microsecond molecular dynamics simulations with AMBER on GPUs. 2. Explicit Solvent Particle Mesh Ewald. J Chem Theory Comput 2013;9:3878–88.
[39] Le Grand S, Götz AW, Walker RC. SPFP: Speed without compromise—A mixed precision model for GPU accelerated molecular dynamics simulations. Comput Phys Commun 2013;184:374–80.
[40] Li P, Merz Jr KM. MCPB.py: A Python Based Metal Center Parameter Builder. J Chem Inf Model 2016;56:599–604.
[41] Wang J, Wolf RM, Caldwell JW, Kollman PA, Case DA. Development and testing of a general amber force field. J Comput Chem 2004;25:1157–74.
[42] Maier JA, Martinez C, Kasavajhala K, Wickstrom L, Hauser KE, Simmerling C. ff14SB: improving the accuracy of protein side chain and backbone parameters from ff99SB. J Chem Theory Comput 2015;11:3696–713.
[43] Roe DR, Cheatham III TE. PTRAJ and CPPTRAJ: software for processing and analysis of molecular dynamics trajectory data. J Chem Theory Comput 2013;9:3084–95.
[44] Chung LW, Sameera WM, Ramozzi R, Page AJ, Hatanaka M, Petrova GP, et al. The ONIOM Method and Its Applications. Chem Rev 2015;115:5678–796.
[45] Sousa SF, Ribeiro AJM, Neves RPP, Brás NF, Cerqueira NMFSA, Fernandes PA, et al. Application of quantum mechanics/molecular mechanics methods in the study of enzymatic reaction mechanisms. WIREs Comput Mol Sci 2016;7:e1281.
[46] Senn HM, Thiel W. QM/MM methods for biomolecular systems. Angew Chem Int Ed Engl 2009;48:1198–229.
[47] Meelua W, Wanjai T, Thinkumrob N, Friedman R, Jitonnom J. Multiscale QM/MM simulations identify the roles of Asp239 and 1-OH…Nucleophile in Transition State Stabilization in Arabidopsis thaliana Cell-Wall Invertase 1. J Chem Inf Model 2023;63:4827–38.
[48] Medina FE, Neves RP, Ramos MJ, Fernandes PA. A QM/MM study of the reaction mechanism of human beta-ketoacyl reductase. Phys Chem Chem Phys 2016;19:347–55.
[49] Mann D, Howeler U, Kotting C, Gerwert K. Elucidation of Single Hydrogen Bonds in GTPases via Experimental and Theoretical Infrared Spectroscopy. Biophys J 2017;112:66–77.
[50] Sharma H, Raju B, Narendra G, Motiwale M, Sharma B, Verma H, et al. QM/MM studies on enzyme catalysis and insight into designing of new inhibitors by ONIOM approach: recent update. ChemistrySelect 2023;8.
[51] Meelua W, Thinkumrob N, Saparpakorn P, Pengthaisong S, Hannongbua S, Ketudat Cairns JR, et al. Structural basis for inhibition of a GH116 beta-glucosidase and its missense mutants by GBA2 inhibitors: crystallographic and quantum chemical study. Chem Biol Inter 2023;384:110717.
[52] Dapprich S, Komáromi I, Byun KS, Morokuma K, Frisch MJ. A new ONIOM implementation in Gaussian98. Part I. The calculation of energies, gradients, vibrational frequencies and electric field derivatives. J Mol Struct: THEOCHEM 1999;461:1–21.
[53] Harris TV, Szilagyi RK. Protein environmental effects on iron-sulfur clusters: a set of rules for constructing computational models for inner and outer coordination spheres. J Comput Chem 2016;37:1681–96.
[54] Kulik HJ, Zhang J, Klinman JP, Martinez TJ. How Large Should the QM Region Be in QM/MM Calculations? The Case of Catechol O-Methyltransferase. J Phys Chem B 2016;120:11381–94.
[55] Vreven T, Frisch M, Kudin K, Schlegel H, Morokuma K. Geometry optimization with QM/MM methods II: Explicit quadratic coupling. Mol Phys 2006;104:701–14.
[56] Yagi K, Ito S, Sugita Y. Exploring the minimum-energy pathways and free-energy profiles of enzymatic reactions with QM/MM Calculations. J Phys Chem B 2021;125:4701–13.
[57] Kreppel A, Ochsenfeld C. The enzymatic decarboxylation mechanism of 5-Carboxy uracil: a comprehensive quantum chemical study. J Chem Theory Comput 2021;17:96–104.
[58] Chai L, Ji S, Zhang S, Yu H, Zhao M, Ji L. Biotransformation Mechanism of Pesticides by Cytochrome P450: A DFT Study on Dieldrin. Chem Res Toxicol 2020;33:1442–8.
[59] Liao R-Z, Zhang J-X, Lin Z, Siegbahn PEM. Antiferromagnetically coupled [Fe8S9] cluster catalyzed acetylene reduction in a nitrogenase-like enzyme DCCPCh: Insights from QM/MM calculations. J Catal 2021;398:67–75.
[60] Song Z, Trozzi F, Tian H, Yin C, Tao P. Mechanistic insights into enzyme catalysis from explaining machine-learned quantum mechanical and molecular mechanical minimum energy pathways. ACS Phys Chem Au 2022;2:316–30.
[61] Magalhães RP, Fernandes HS, Sousa SF. Modelling enzymatic mechanisms with QM/MM approaches: current status and future challenges. Isr J Chem 2020;60:655–66.
[62] Cee VJ, Volak LP, Chen Y, Bartberger MD, Tegley C, Arvedson T, et al. Systematic Study of the Glutathione (GSH) Reactivity of N-Arylacrylamides: 1. Effects of Aryl Substitution. J Med Chem 2015;58:9171–8.
[63] Shin Y, Jeong JW, Wurz RP, Achanta P, Arvedson T, Bartberger MD, et al. , Discovery of N-(1-Acryloylazetidin-3-yl)-2-(1H-indol-1-yl)acetamides as Covalent Inhibitors of KRAS(G12C). ACS Med Chem Lett 2019;10:1302–8.
[64] Arnold AP, Canty AJ. Methylmercury (II) sulfhydryl interactions. Potentiometric determination of the formation constants for complexation of methylmercury (II) by sulfhydryl containing amino acids and related molecules, including glutathione. Can J Chem 1983;61:1428–34.
[65] Lang X, Lyubovitsky JG. Structural dependency of collagen fibers on ion types revealed by in situ second harmonic generation (SHG) imaging method. Anal Methods 2015;7:1680–90.
[66] Singh J, Petter RC, Baillie TA, Whitty A. The resurgence of covalent drugs. Nat Rev Drug Discov 2011;10:307–17.
[67] Baillie TA. Targeted covalent inhibitors for drug design. Angew Chem Int Ed Engl 2016;55:13408–21.
[68] Dutta, N.; Saha, M.K. Chapter Nine - Immobilization of a Mesophilic Lipase on Graphene Oxide: Stability, Activity, and Reusability Insights. In Methods in Enzymology, Kumar, C. V., Ed.; Academic Press: 2018; Vol. 609, pp 247–272.
[69] Burlingham BT, Widlanski TS. An intuitive look at the relationship of Ki and IC50: a more general use for the Dixon plot. J Chem Educ 2003;80:214.
[70] Kim H, Hwang YS, Kim M, Park SB. Recent advances in the development of covalent inhibitors. RSC Med Chem 2021;12:1037–45.